Article

Recurrent Supramolecular Patterns in a Series of Salts of Heterocyclic Polyamines and Heterocyclic Dicarboxylic Acids: Synthesis, Single-Crystal X-ray Structure, Hirshfeld Surface Analysis, Energy Framework, and Quantum Chemical Calculations

Joanna Bojarska [1,*], Krzysztof Łyczko [2], Martin Breza [3] and Adam Mieczkowski [4,*]

1   Institute of General and Ecological Chemistry, Faculty of Chemistry, Lodz University of Technology, Zeromskiego 116, 90-924 Lodz, Poland
2   Institute of Nuclear Chemistry and Technology, Dorodna 16, 03-195 Warsaw, Poland; k.lyczko@ichtj.waw.pl
3   Department of Physical Chemistry, Slovak Technical University, Radlinskeho 9, SK-81237 Bratislava, Slovakia; martin.breza@stuba.sk
4   Institute of Biochemistry and Biophysics, Polish Academy of Sciences, Pawinskiego 5a, 02-106 Warsaw, Poland
*   Correspondence: joanna.bojarska@p.lodz.pl (J.B.); amiecz@ibb.waw.pl (A.M.)

Abstract: A series of novel salts based on aromatic polyamines and 2,3-pyrazinedicarboxylic acid, such as $C_{10}H_{12}N_6O_5$ (**1**), $C_{10}H_9ClN_6O_4$ (**2**), $C_{11}H_{10}N_8O_4$ (**3**), and $C_{14}H_{17}N_{16}O_{5.5}$ (**4**) or 3,4-thiophenedicarboxylic acid, such as $C_{10}H_{10}N_4O_4S$ (**5**), $C_{10}H_9ClN_4O_4S$ (**6**), and $C_{10}H_{10}N_4O_4S_2$ (**7**), were synthesized and characterized by single-crystal X-ray diffraction. All compounds crystallize in a monoclinic space group. The structure was subjected to complex Hirshfeld surface analysis, molecular electrostatic potential, enrichment ratio, and energy framework calculations. The influence of different cations on the packing of 3-carboxypyrazine-2-carboxylate and 4-carboxythiophene-3-carboxylate anions in the crystal lattice was studied. $O\cdots H/H\cdots O$ interactions are the main contributor in all crystals. In addition, in a series of pyrazine-containing structures, $N(C)\cdots H/H\cdots N(C)$ interactions have relevance, while in a series of thiophene-based compounds, $C\cdots H/H\cdots C$ and $S\cdots H(O)/H(O)\cdots S$. In addition, Cl-based interactions are observed in compound **2**. According to the enrichment ratio calculations, $O\cdots H/H\cdots O$ and $C\cdots C$ are the most preferable interactions in all structures. The energy frameworks are dominated by the dispersive contribution, only in compound **3** is the electrostatic term dominant. The analyzed structures reveal intra- and intermolecular recurrent supramolecular synthons. In both series of crystals, the robust H-bonded centrosymmetric dimer $R^2_2(8)$ as homo- or as heterosynthon (in compounds **2**, **3**, **6**, and **7**) and the intramolecular synthon $S(7)$ generated by O-H$\cdots$O interactions (in compounds **2**, **6**, and **7**) are present. The supramolecular patterns formed by $\pi\cdots\pi$ ($C\cdots C$) and C-O(Cl,S)$\cdots$C are also noticeable. Notably, a dual synthon linking the supramolecular chain via $\pi\cdots\pi$ interactions and the homosynthon $R^2_2(8)$ via N-H$\cdots$N interactions is visible in both series of new salts. A library of H-bonding motifs at diverse levels of supramolecular architecture is provided. We extended the analysis of intramolecular H-bonding motifs to similar structures deposited in the Cambridge Structural Database. Another important feature is the existence of an intramolecular $O\cdots H\cdots O$ bridge between two neighboring carboxylic groups as substituents in anions in compounds **3** and **5**. In this context, we performed quantum theory of atoms-in-molecule calculations to reveal more details.

Keywords: thiophene; pyrimidine; pyrazine; crystal structure; supramolecular synthon; Hirshfeld surface; molecular electrostatic potential; enrichment ratio; energy frameworks; QTAIM

1. Introduction

Several salts of 3-carboxypyrazine-2-carboxylate anion with various organic cations, including 2-amino-5-bromo-6-methyl-4-oxo-3,4-dihydropyrimidin-1-ium [1], 2-amino-6-methyl-4-oxo-3,4-dihydropyrimidin-1-ium [2], pyridinium derivatives [3,4], 1,2,4-triazolium derivatives [5,6], carboxyphenylammonium [6,7], L-tryptophanium [8], 4-carbamoylpiperidinium [9], 8-hydroxyquinolinium [10], acridinium [11], 1,4-diazoniacyclohexane [12], and 7-amino-2,4-dimethyl-1,8-naphthyridin-1-ium [13], are presented. In addition, only a few structures of metal complexes with the 4-carboxythiophene-3-carboxylate anion acting as a ligand or counterion are known [14–19]. Salts of this anion with organic cations have not been structurally studied so far.

Crystal engineering is an important and emerging part of crystallography with special importance in the development of pharmaceutical co-crystals [20,21], metal–organic frameworks (MOFs) [22,23], and catalysis [24]. In this paper, as a continuation of our crystal engineering and supramolecular studies on the organic compounds [25,26], we present the synthesis and supramolecular characterization of two series of new salts based on aromatic polyamines and 2,3-pyrazinedicarboxylic acid, such as 2,4-diaminopyrimidin-1-ium 3-carboxypyrazine-2-carboxylate hydrate (**1**), 2,4-diamino-6-chloropyrimidin-3-ium 3-carboxypyrazine-2-carboxylate (**2**), 2,6-diaminopurin-1-ium 3-carboxypyrazine-2-carboxylate (**3**), and 2,6-diamino-5-azapurin-9-ium 3-carboxypyrazine-2-carboxylate 2,6-diamino-5-azapurine sesquihydrate (**4**), and 3,4-thiophenedicarboxylic acid, such as 2,4-diaminopyrimidin-1-ium 4-carboxythiophene-3-carboxylate (**5**), 2,4-diaminopyrimidin-3-ium 4-carboxythiophene-3-carboxylate (**6**), and 4,6-diamino-2-thiopyrimidin-1-dium 4-carboxythiophene-3-carboxylate (**7**) (Figure 1). We focus on examining the nature and hierarchy of noncovalent interactions participating in the formation of recurrent supramolecular hydrogen bonding and π-based patterns. Insight into these properties is obtained using full interaction maps and complex Hirshfeld surface analysis, including 3D Hirshfeld maps and molecular electrostatic potentials mapped on the Hirshfeld surfaces, 2D fingerprint plots and enrichment ratios, as well as energy frameworks. The structural specificity of the new salts resulted from the neighboring two carboxylic groups, which can generate the intramolecular O⋯H⋯O bridge. It is worth mentioning the negative charge of one of the carboxylate groups by which charge-assisted hydrogen bonds are formed. In this context, experimental findings are corroborated via quantum chemical calculations to reveal more details. Moreover, given the tendency of new salts to participate in the formation of recurrent robust intramolecular synthons, we decided to more closely investigate the supramolecular behavior of similar structures deposited in the Cambridge Structural Database (CSD version 5.43, updated May 2024) [27]. In the further context of supramolecular aspects of new salts, enriched 3D networks in classical or nonclassical interactions are observed. Therefore, we developed a hierarchical library of H-bonding motifs at various levels of supramolecular architecture and describe π-based supramolecular motifs.
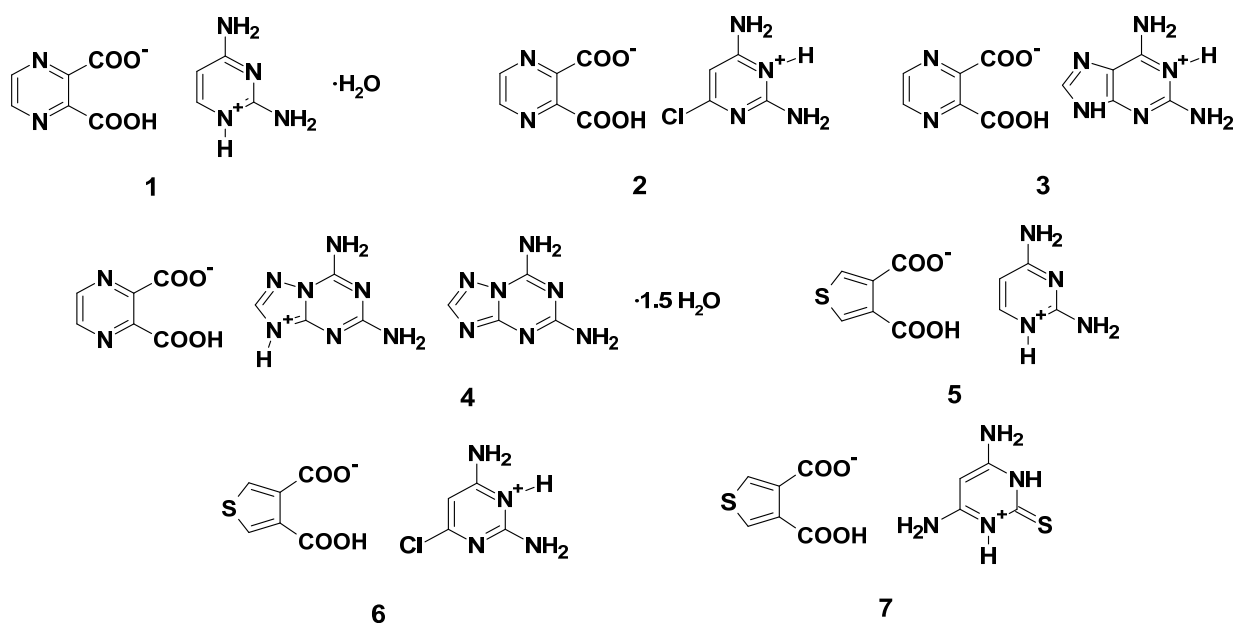
Figure 1. Structure of analyzed salts: 2,4-diaminopyrimidin-1-ium 3-carboxypyrazine-2-carboxylate monohydrate (**1**), 2,4-diamino-6-chloropyrimidin-3-ium 3-carboxypyrazine-2-carboxylate (**2**), 2,6-diaminopurin-1-ium 3-carboxypyrazine-2-carboxylate (**3**), 2,6-diamino-5-azapurin-9-ium 3-carboxypyrazine-2-carboxylate 2,6-diamino-5-azapurine sesquihydrate (**4**), 2,4-diaminopyrimidin-1-ium 4-carboxythiophene-3-carboxylate (**5**), 2,4-diaminopyrimidin-3-ium 4-carboxythiophene-3-carboxylate (**6**), 4,6-diamino-2-thiopyrimidin-1-dium 4-carboxythiophene-3-carboxylate (**7**).

2. Materials and Methods

2.1. Synthesis of Compounds **1–7**

The commercially available chemicals were of reagent grade and used as received. 2,6-diamino-5-azapurine was synthesized according to a literature procedure [28]. The infrared spectra for studied compounds were recorded on a ZnSe crystal using the ATR technique and a Thermo Scientific Nicolet iS10 FTIR spectrometer. The following procedure was applied to obtain the requested crystals of heterocyclic polyamines and aromatic dicarboxylic acids.

Synthesis of salts of 2,3-pyrazinedicarboxylic acid **1–4**

2,3-pyrazinedicarboxylic acid (0.1 mmol, 1 equiv, 17 mg) and appropriate organic diamine (0.1 mmol, 1 equiv., 11 mg of 2,4-diaminopyrimidine; 15 mg of 2,4-diamino-6-chloropyrimidine; 15 mg of 2,6-diaminopurine; 15 mg of 2,6-diamino-5-azapurine) were dissolved/dispersed in 2 mL of warm distilled water (~80 °C), cooled to room temperature with stirring, then filtered through a small cotton pad and left at room temperature for crystallization (about 2 weeks). The obtained salts' crystals were used for the X-ray measurements and recording of the ATR-FTIR spectra.

Compound **1**: ATR-FTIR (ZnSe), ν_{max}/cm^{-1}: 3347 s (N–H), 3162 s (N–H), 3059 sh (N–H), 2985 m, 3039 w, 2952 w, 1654 s (C=O), 1617 vs (C=O), 1567 sh, 1512 s, 1449 m, 1380 m, 1274 m, 1247 sh, 1216 m, 1184 m, 1163 m, 1100 m, 1072 sh, 1060 m, 981 w, 870 m, 839 w, 802 m, 786 m, 768 m, 712 m.

Compound **2**: ATR-FTIR (ZnSe), ν_{max}/cm^{-1}: 3430 w (N–H), 3275 sh (N–H), 3226 sh (N–H), 3129 s (N–H), 3114 sh (N–H), 3050 sh, 2580 w vbr, 1672 s (C=O), 1635 s (C=O), 1560 sh, 1537 sh, 1495 vs, 1472 sh, 1408 m, 1389 m, 1371 sh, 1357 s, 1285 m, 1203 m, 1162 m, 1127 w, 1091 m, 1057 m, 1034 m, 978 m, 935 w, 906 w, 875 m, 818 m, 765 m, 755 m, 727 w, 680 m.

Compound **3**: ATR-FTIR (ZnSe), ν_{max}/cm^{-1}: 3419 m (N–H), 3303 w (N–H), 3255 w (N–H), 3125 sh (N–H), 3110 sh (N–H), 3033 m vbr, 2911 w, 2837 w vbr, 2708 w vbr, 1698 sh (C=O), 1684 sh (C=O), 1654 vs (C=O), 1651 sh (C=O), 1610 m, 1544 s, 1507 s, 1473 sh, 1443 vs, 1418 sh, 1385 m, 1332 s, 1296 m, 1224 m, 1170 m, 1142 m, 1119 sh, 1085 m, 1043 m, 964 m, 904 w, 890 w sh, 883 w, 842 m, 812 m, 765 s, 756 sh, 721 w.

Compound **4**: ATR-FTIR (ZnSe), ν_{max}/cm^{-1}: 3616 w (N–H), 3513 w (N–H), 3455 w (N–H), 3308 m br (N–H), 3246 m br (N–H), 3150 m (N–H), 3060 m br, 2909 w, 1685 s (C=O), 1645 vs (C=O), 1622 sh, 1575 sh, 1553 s, 1530 sh, 1512 m, 1456 m, 1441 m, 1392 m, 1368 m, 1326 m, 1271 m, 1251 sh, 1221 m, 1186 w, 1166 m, 1142 m, 1107 m, 1073 sh, 1054 sh, 1005 w, 918 m, 898 sh, 876 m, 841 w, 805 w, 780 m, 764 m, 724 m, 697 m, 679 m.

Synthesis of salts of 3,4-thiophenedicarboxylic acid **5**–**7**

3,4-thiophenedicarboxylic acid (0.1 mmol, 1 equiv., 17 mg) and appropriate organic diamine (0.1 mmol, 1 equiv., 11 mg of 2,4-diaminopyrimidine; 15 mg of 2,4-diamino-6-chloropyrimidine; 16 mg of 4,6-diamino-2-thiopyrimidine hydrate) were dissolved/dispersed in 2 mL of warm distilled water (~80 °C), cooled to room temperature with stirring, then filtered through a small cotton pad and left at room temperature for crystallization (about two weeks). The obtained salts' crystals were used for the X-ray measurements and recording of the ATR-FTIR spectra.

Compound **5**: ATR-FTIR (ZnSe), ν_{max}/cm^{-1}: 3450 m (N–H), 3292 m br (N–H), 3400 sh (N–H), 3124 s (N–H), 2943 w, 2910 w, 2872 w, 2808 w, 2736 w br, 2624 w br, 1713 m (C=O), 1701 sh (C=O), 1649 s (C=O), 1589 w, 1511 vs, 1436 s, 1398 sh, 1372 s, 1325 s, 1234 m, 1168 m, 1076 w br, 1013 m, 980 sh, 965 m, 880 m, 864 sh, 831 w, 800 m, 784 w, 758 m, 716 w.

Compound **6**: ATR-FTIR (ZnSe), ν_{max}/cm^{-1}: 3418 m (N–H), 3303 w br (N–H), 3255 sh (N–H), 3125 m (N–H), 3110 m (N–H), 3040 m vbr, 1681 sh (C=O), 1654 s (C=O), 1611 m, 1546 s, 1512 s, 1475 m, 1443 vs, 1419 sh, 1385 m, 1333 s, 1296 m, 1225 m, 1170 m, 1144 m, 1119 sh, 1087 m, 1043 m, 966 m, 890 w, 883 w, 842 m, 812 m, 765 s,

Compound **7**: ATR-FTIR (ZnSe), ν_{max}/cm^{-1}: 3379 w (N–H), 3322 w vbr (N–H), 3199 sh (N–H), 3105 m vbr (N–H), 3010 m vbr, 2771 w vbr, 1658 s (C=O), 1632 sh v, 1557 m, 1551 sh, 1486 vs, 1441 s, 1386 m, 1336 m, 1284 sh, 1272 m, 1178 s, 1157 sh, 1121 m, 1035 w, 1015 w, 960 w, 901 w, 840 m, 768 m, 657 m.

2.2. Single-Crystal X-ray Diffraction

Diffraction data were collected at low temperatures on a Rigaku SuperNova (dual source) four-circle diffractometer equipped with an Eos CCD detector using a mirror-monochromated Cu Kα radiation (λ = 1.54184 Å) from a microfocus Nova X-ray source. CrysAlis Pro software (version CrysAlisPro 1.171.41.112a) was used to perform all necessary operations, including data collection, their reduction, and multi-scan absorption correction. The crystal structures were solved and refined by a direct method and a full-matrix least-squares treatment on F^2 data. Anisotropic atomic displacement parameters were applied for all non-hydrogen atoms during the refinement procedure. The positions of the major hydrogen atoms bonded to the oxygen and nitrogen atoms were found in a difference Fourier map and freely refined. The remaining H atoms were placed in idealized positions using standard parameters. All hydrogens were refined isotropically. All calculations were performed using SHELXTL programs [29], operating within the OLEX2 crystallographic software (version 1.3) [30]. Graphic images and analysis of the structures were prepared with the Mercury (version 2023.3.1) [31] and PLATON (version 2023.1) [32] programs. All crystal structures have been deposited in the CSD (CSD 2364043–2364049 for **1**–**7**).

2.3. Computational Details

2.3.1. Quantum Chemical Calculations

The geometry of 4-carboxythiophene-3-carboxylate (**A**$^-$) and 3-carboxypyrazine-2-carboxylate (**B**$^-$) anions in ground singlet spin states was completely optimized using Gaussian 09 software (version D.01) [33]. The MP2 method [34–36] and the 6–311++G(d,p) basis sets for all atoms from the Gaussian library [34] were employed. The optimized

geometries were checked for the absence of imaginary vibrations by vibrational analysis. The electron structures of the optimized systems were compared in terms of Quantum Theory of Atoms-in-Molecules (QTAIM) [37] using AIM2000 software (version 1.0) [38]. The bond strengths were discussed in terms of the electron densities ρ_{BCP} and the bond characteristics in terms of their electron density Laplacians $\nabla^2\rho_{BCP}$ (negative values for covalent bonds) at their bond-critical points (BCP). The BCP bond ellipticities ε_{BCP} are defined as:

$$\varepsilon_{BCP} = \lambda_1/\lambda_2 - 1 \tag{1}$$

where $\lambda_1 < \lambda_2 < 0 < \lambda_3$ are the eigenvalues of the Hessian of the BCP electron density. Atomic charges were obtained by integration of the electron density within their atomic basins (up to the 0.001 e/Bohr^3 isosurface).

2.3.2. Hirshfeld Surface Analysis and Energy Frameworks

The CrystalExplorer program (ver. 21.5) was used to perform complex Hirshfeld surface analysis, including 3D surface maps [39,40] and 2D fingerprint plots [40], as well as molecular electrostatic potentials [41,42] utilizing CIF files of **1–7** collected from the X-ray experiments. The bond lengths of the hydrogen atoms were normalized to standard neutron diffraction values [43]. The molecular electrostatic potential mapped onto Hirshfeld surfaces was generated at the wave function of the HF/STO-3G level using CrystalExplorer [41,42]. In addition, pairwise interaction energies were calculated using Tonto within a 3.8 Å radius around the main molecule at the B3LYP/6-31G(d,p) level of theory [44]. The default scaling factors reported by Mackenzie et al. were applied [45]. The enrichment ratios (ER) of the close interactions in crystals **1–7** were calculated based on the HS results [46]. Full interaction maps (FIMs) were calculated for **1–7** based on CSD interaction data [47] using the Mercury program [31].

2.3.3. CSD Search

A search of CSD (version 5.43 updates March 2024) [27] was conducted using dicarboxylic-pyrazine/thiophene scaffolds. Notably, the findings confirmed the synthesized compounds' **1–7** novelty. Next, we restricted the survey to the following filters: *R* factor ≤ 0.05, no errors, not polymeric, only organics, only non-disordered, only single crystal structures, no repeated entries, and 3D coordinates determined. As a result, pyrazine-based compounds, such as *L*-tryptophanium (hydrogen 2,3-pyrazinedicarboxylate) dihydrate (CSD ref. code: BEBCET) [8], 3-carboxyphenylammonium hydrogen 2,3-pyrazinedicarboxylate dihydrate (ZIKREQ) [7], 4-((2-carbamoylhydrazineylidene)methyl)pyridin-1-ium 3-carboxypyrazine-2-carboxylate (LOFQIJ) [4], pyrazine-2,3-dicarboxylic acid 4-aminobenzoic acid (LEJRIB) [6], 2-amino-5-bromo-6-methyl-4-oxo-3,4-dihydropyrimidin-1-ium 3-carboxypyrazine-2-carboxylate 2-amino-5-bromo-6-methylpyrimidin-4(1*H*)-one monohydrate (DIMNAR) [1], 2-imino-1-methyl-1,5-dihydro-4*H*-imidazol-4-one pyrazine-2,3-dicarboxylic acid (MIPWEN) [48], and 2,4-diazoniacyclohexane bis(3-carboxypyrazine-2-carboxylate) dihydrate (VUZYUL) [12], and molecules containing carboxy-thiophene, such as diaqua-bis(1,10-phenanthroline)-zinc(ii) bis(4-carboxythiophene-3-carboxylate) heptahydrate (LUDTAH) [14], catena-[(μ$_2$-4,4′-bipyridine)-bis(μ$_2$-thiophene-3,4-dicarboxylato)-cadmium(II)] (NIBPIZ) [15], and bis(2,2′-bipyridine)-bis(thiophene-3,4-dicarboxylato)-cadmium(II) (WUVCUN01) [16], were included in the analysis. The structural formulas of these species are presented in Table S1 in Supporting Information.

3. Results and Discussion

### 3.1. Crystal Structures and Hirshfeld Surface Analysis

The crystal structures of **1–7** were determined by single-crystal X-ray diffraction at low temperatures with the highest precision. All structures crystallize in the monoclinic system, in achiral space groups. In all cases, the asymmetric unit comprises one cation and one anion. In addition, compounds **1** and **4** crystallize with water solvent molecules. All bond lengths and angles fall within normal ranges. Selected crystallographic data and

refinement details are given in Table S2, the molecular structures are presented in Figures 2 and 3, and the geometric parameters of H-bonding interactions are summarized in Table S3. We performed a quantitative analysis of the crystal packing of new salts by calculating the Kitaigorodsky packing index (KPI) [49,50] using the "calc void" procedure in the PLATON program [32]. The results revealed that **2** is the most and **6** is the least closely packed crystal structure, with 76.2% and 69.9% of filled space, respectively. No space accessible for voids was found (Table 1). In all crystal structures, O-H⋯O, N-H⋯O, and C-H⋯O hydrogen bonds are present, where the shortest H⋯A distance is 1.57 Å for O-H⋯O in **1**, 1.65 Å for N-H⋯O in **4**, and 2.37 Å for C-H⋯O in **1**. Moreover, N-H⋯N interactions exist in almost all structures (apart from **5** and **7**), C-H⋯N in **1**, **2**, **3**, and **5**, O-H⋯N in **4**, while N-H⋯S exists in **5** and **7**. Furthermore, the presence of different types of cations and their substituents predetermine how crystal structures are stabilized by π-based interactions, which are summarized in the Supporting Information in Tables S4 and S5, including the inter-centroid distances, slip angles, dihedral angles between the centroid vector and normal to the ring plane, dihedral angles between planes, perpendicular distance of centroids on rings, and all lengths between ring centroids. In particular, π⋯π (C⋯C) (Cg⋯Cg distance below 4 Å) interactions are observed in **3**, **4**, and **5**, C-Cl⋯C in **2**, C-S⋯C in **7**, and C-O⋯C in all crystals, apart from **1** and **5**.
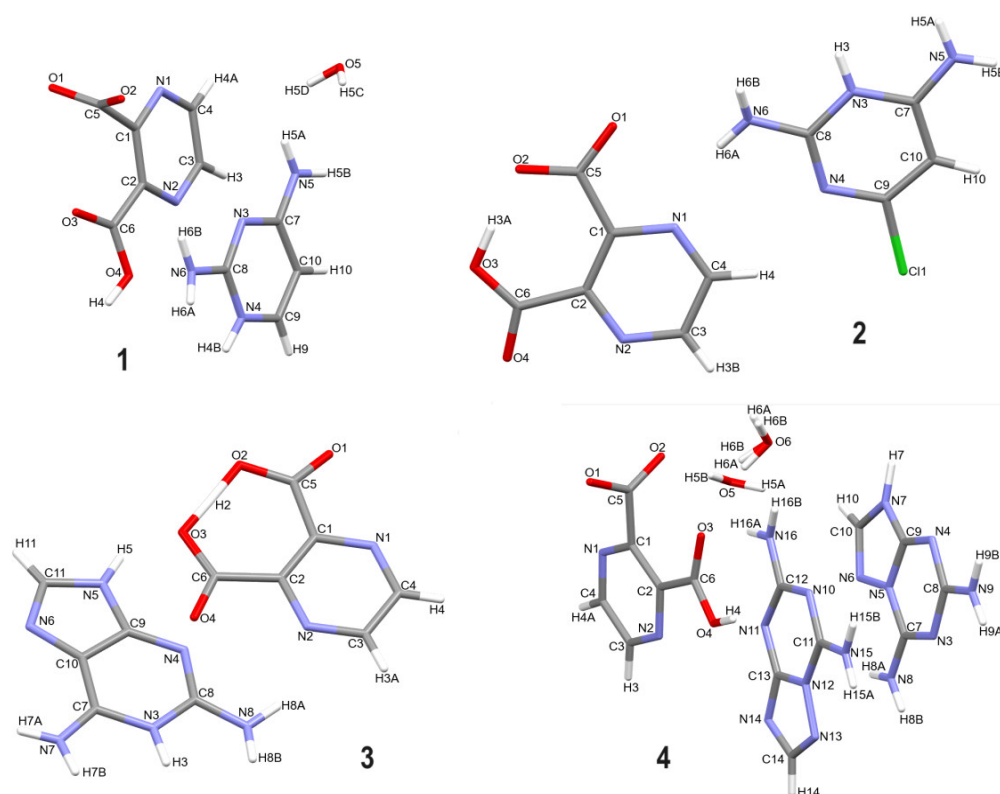
**Figure 2.** Molecular structures of **1–4** showing the atom numbering scheme.
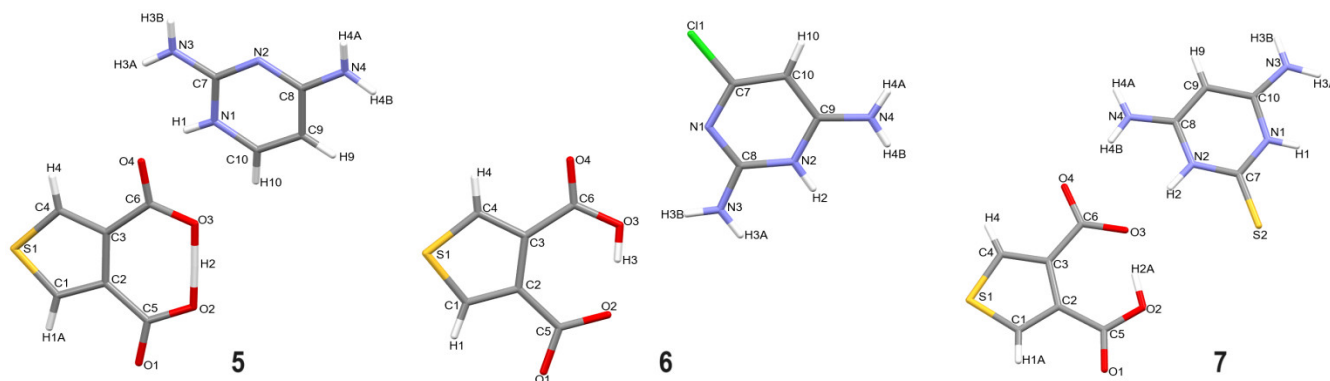
Figure 3. Molecular structures of **5**–**7** showing the atom numbering scheme.

Table 1. Summarized total energies kJ/mol for crystals **1**–**7** according to the energy framework calculations.

Crystal	E_{ele}	E_{pol}	E_{dis}	E_{rep}	E_{tot}
1	−44.4	−36	−100.1	233.8	46.6
2	−129.7	−37.6	−183.9	218.2	−145.2
3	−76.5	−32.3	−61.7	44.2	−118.4
4	−54.5	−13.7	−107.1	125.4	−58.8
5	105.6	−51.8	−114.5	72.3	36.9
6	−60.7	−32.6	−111	200.4	−20.2
7	−23.7	−40	−83.2	43.1	−89.8

To gain deeper insight into the nature of noncovalent interactions and the relevance of the corresponding types of close contacts in supramolecular structures **1**–**7**, a complex Hirshfeld surface analysis was performed. The percentage contributions of diverse close intercontacts to the Hirshfeld surfaces of **1**–**7** crystals are shown in Figure 4. It should be highlighted that O⋯H/H⋯O, C⋯H/H⋯C, and H⋯H interactions are present in all structures. More specifically, O⋯H/H⋯O interactions contribute from 49.1% in **1** to 33.4% in **6**, C⋯H/H⋯C from 16.6% in **6** to 7.5% in **5**, and H⋯H from 18.6% in **5** to 8.4% in **3**. Moreover, N⋯H/H⋯N are the next most significant contributors in **1**, **2**, **3**, and **4**—from 26% in **4** to 11.9% in **1**. Notably, C⋯C (π⋯π) interactions have relevance in nearly all structures, apart from **1**—from 8.2% in **5** to 1.4% in **4**. Moving forward, C⋯O/O⋯C (π⋯lone pair/lone pair⋯π) also contribute in all structures (apart from **4**) from 9.6% in **2** to 2% in **1**, while O⋯O (lone pair⋯lone pair), in the majority (apart from **1** and **4**), from 3% in **3** to 1.5% in **2**. In addition, Cl⋯O/O⋯Cl intercontacts are present in **2** and **6** at the level of 3%, S⋯S in **7** (5%), and S⋯H/H⋯S in **5**, **6**, and **7** (~10%) (Figure 5, Table S6). The latter specific Cl- and S-based interactions resulted from the corresponding substituent in cations. They play the role of an additional stabilizer of the crystal structures. Notably, the strongest π⋯π interaction (distance between centroids—3.4639 Å) was found in **4** and C-O⋯C in **3** (3.0860 Å). According to the enrichment ratio calculations based on the Hirshfeld surface analysis, O⋯/H⋯O and C⋯C are the most preferable in nearly all structures. Interestingly, O⋯C/C⋯O interactions are preferable only in **2** and C⋯H/H⋯C—only in **4**. N⋯H/H⋯N are preferable in **2**, **3**, and **4**. Cl-based contacts are preferred in **2** and **6** and S-based in **5**–**7** (Figure 4 and Table S7).
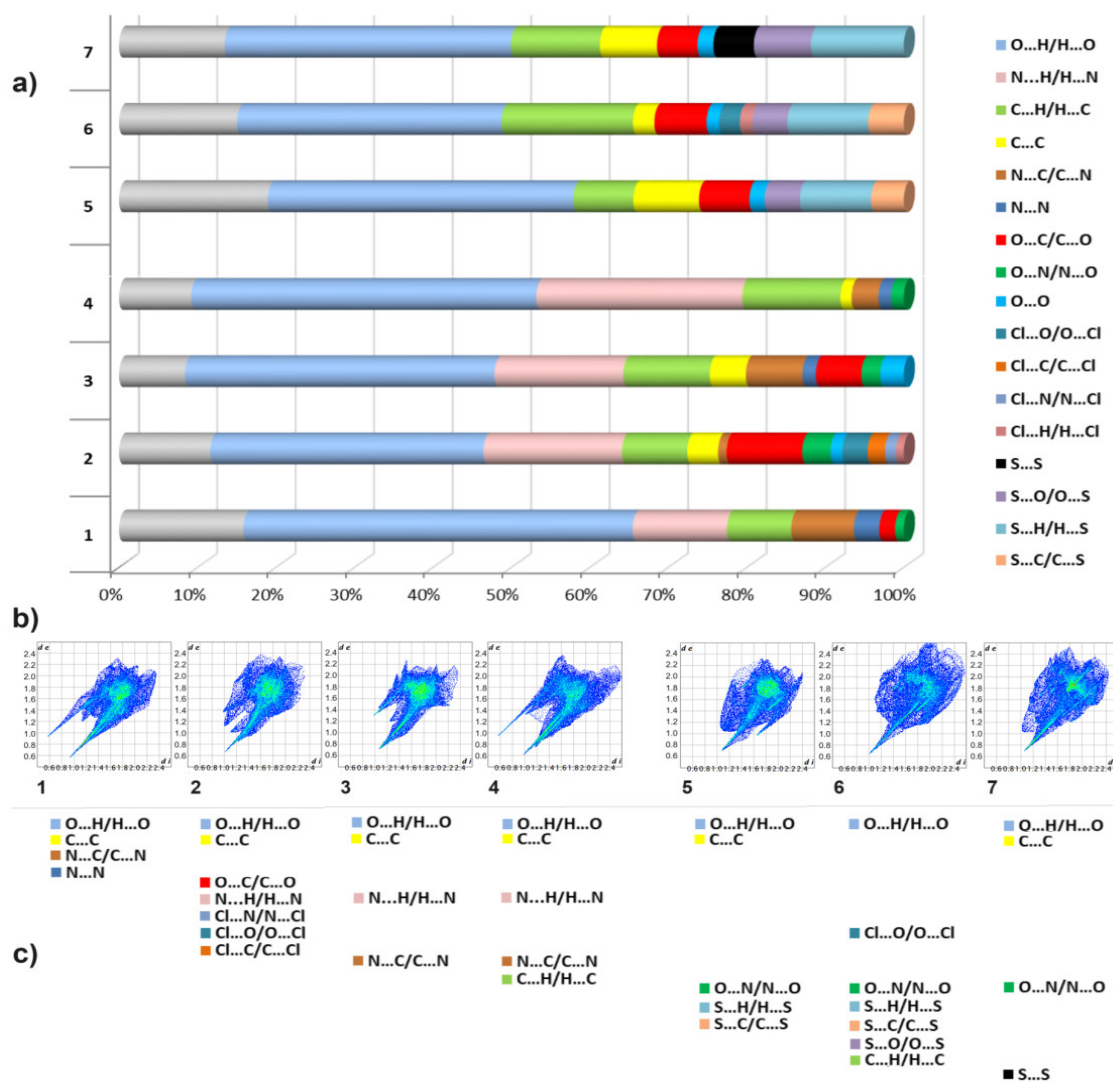
Figure 4. (**a**) Percentage contributions of intercontacts in crystals **1**–**7** (above 1%); (**b**) fingerprint plots for overall interactions for **1**–**7**; (**c**) preferable intercontacts (greater than unity) in **1**–**7** according to the enrichment ratio calculations.
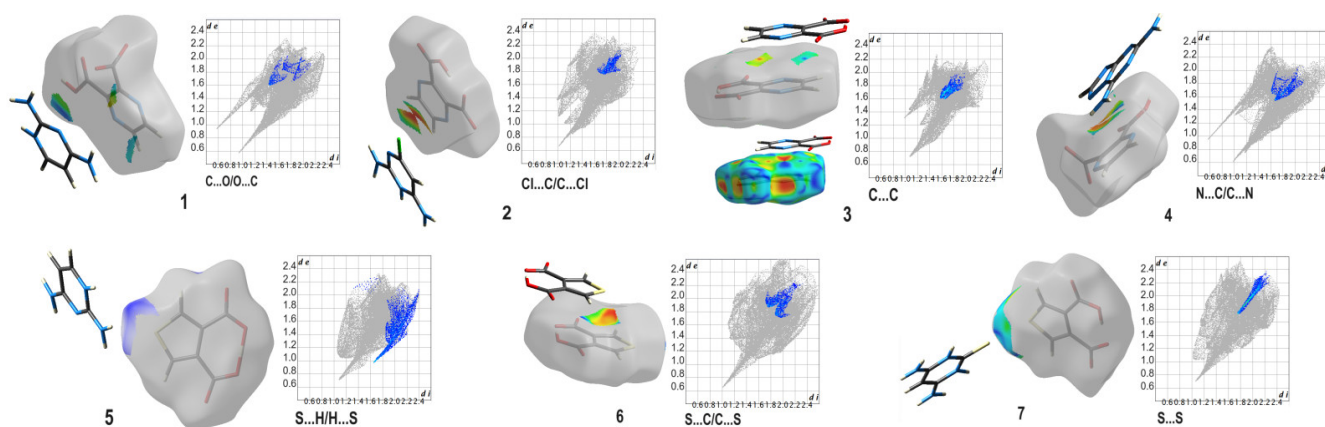

Figure 5. Selected close weak interactions in analyzed salts visualized in the Hirshfeld surface mapsand 2D fingerprint plots.

3.2. Supramolecular Features of **1–7**

At first glance, the supramolecular architecture seems to be similar in **2** and **3** (Figure 6) as well as in **5** and **6** (Figure 7). However, the arrangement of supramolecular H-bonding synthons is different, especially in thiophene-based sulfur-containing structures. Notably, it is reflected in energy frameworks (see section below).
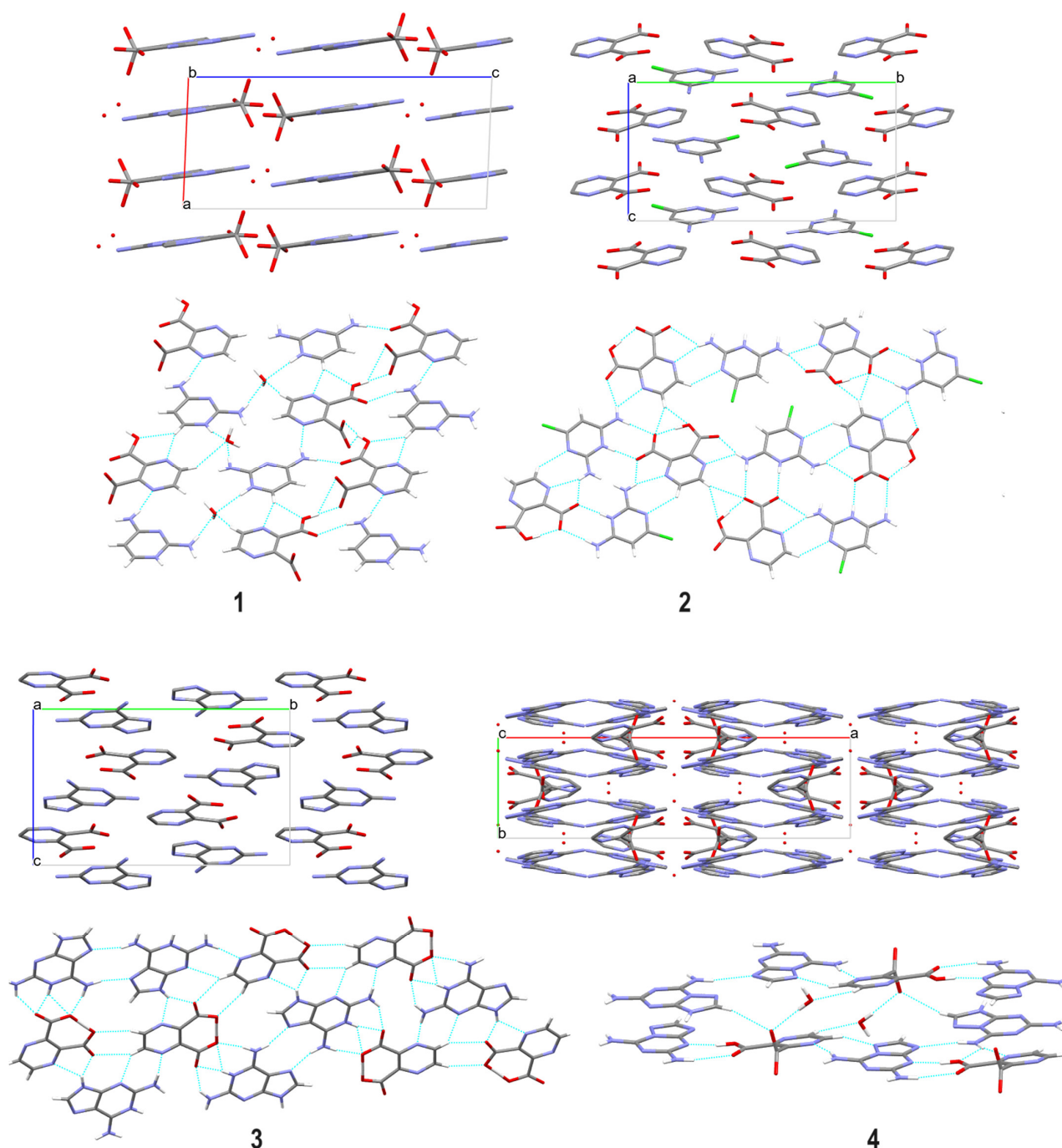

Figure 6. Fragments of the crystal structure **1–4** showing the intermolecular interactions between neighboring molecules.

Both series of novel crystals show the diversity of H-bonding motifs using Etter and Bernstein's graph set notation [51,52]. All types of supramolecular patterns, either intra- (self-motif called *S*) or intermolecular (finite dimer *D*, cyclic motif-ring *R*, and chains *C*), were found [53]. A library of H-bonding synthons observed in crystals **1–7** is provided in

Table S8. Among many H-bonding motifs, we managed to recognize recurrent synthons. To be more precise, the $R^2_2(8)$ homosynthon via N-H···O is the most common synthon (observed in **2**, **3**, **6**, and **7**). The highest number of the same synthons is observed in the crystal lattice of **2** and **3**. In particular, $R^2_1(5)$ with employed bifurcated donor, homodimer $R^2_2(7)$, heterodimer $R^2_2(8)$, and heterotetramers $R^4_4(18)$ and $R^4_4(20)$ (Figure 8, Table S9). On the other hand, in **5** and **6**, only one common synthon is observed, namely, the homodimer $R^2_2(8)$. At the first level of graph-set theory [44], we observed $S(7)$ in **2**, **6**, **7**, and homosynthon $R^2_2(8)$ via N-H···N interactions in **4**, **5**, and **6**. At the second level, the robust synthon $R^2_2(8)$ present in **2**, **3**, **6**, and **7** as a heterosynthon through N-H···O interactions between the NH and COO$^-$ group is worth mentioning (Table S9).
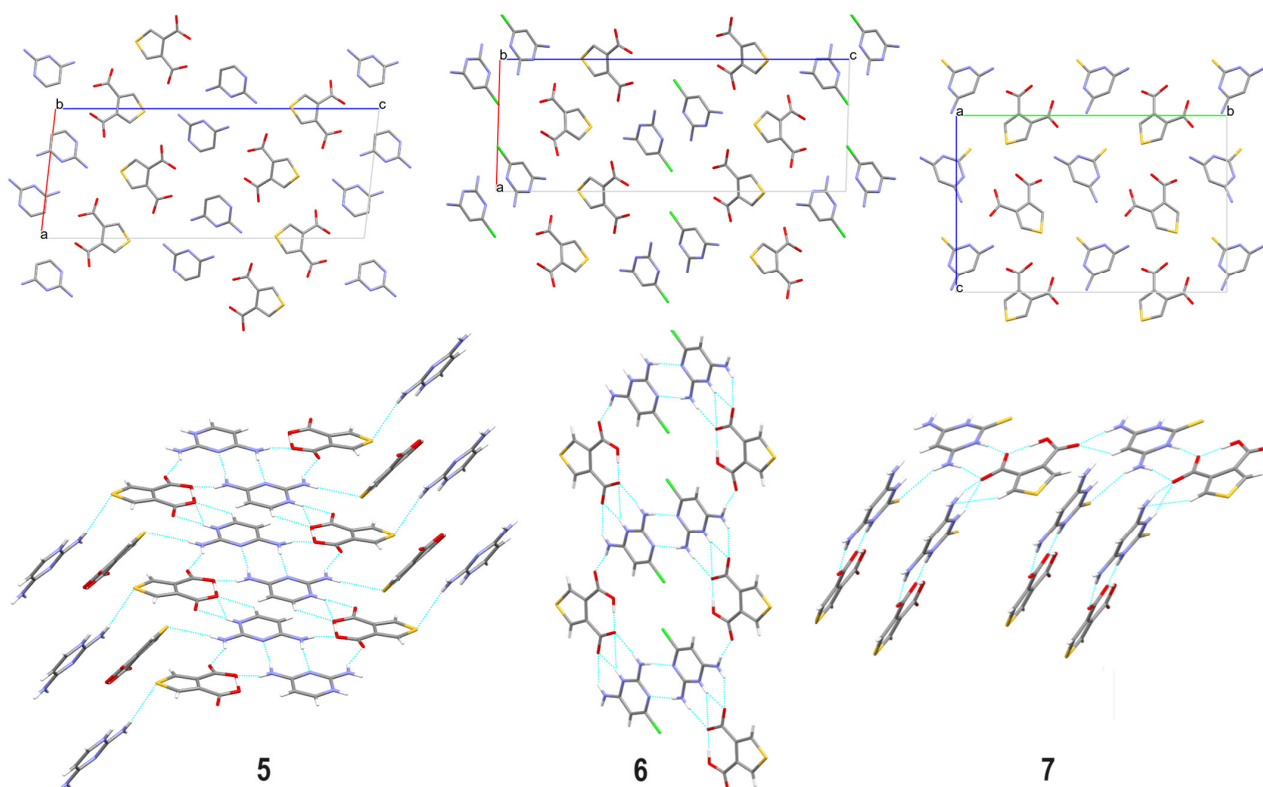
Figure 7. Fragments of the crystal structure **5**–**7** showing the intermolecular interactions between neighboring molecules.

It should be mentioned that the Hirshfeld surface analysis [40] was helpful either in the complex exploration of the noncovalent interactions between neighboring species in the crystal packing of the analyzed compounds or in the identification and visualization of subtle differences in intramolecular interactions. The latter case is elegantly presented mainly by molecular electrostatic potentials mapped on the Hirshfeld surfaces. However, Hirshfeld surfaces with d_{norm}, d_i, d_e and fragment patch properties are also relevant (Figure 9). As an example, on the molecular electrostatic potential mapped on the Hirshfeld surface of crystal **3** (in which the intramolecular O···H···O bridge is formed), the strongest negative electrostatic potential (red region) is observed. A similar situation exists in the second series of new salts containing a thiophene ring (Figure S1). Inspection indicates that EP distribution follows the expected behavior in the corresponding crystals: a clear sigma hole near the oxygen atom of the carbonyl group in **1** without intramolecular interactions, a small sigma hole between carboxylic groups in **2**, where the intramolecular synthon, denoted S(7) is formed, and no sigma hole in **3**, in which the intramolecular O···H···O bridge is generated (yellow circles). This situation proves that Hirshfeld surface analysis is also suitable for identifying supramolecular nuances related to intramolecular interactions.
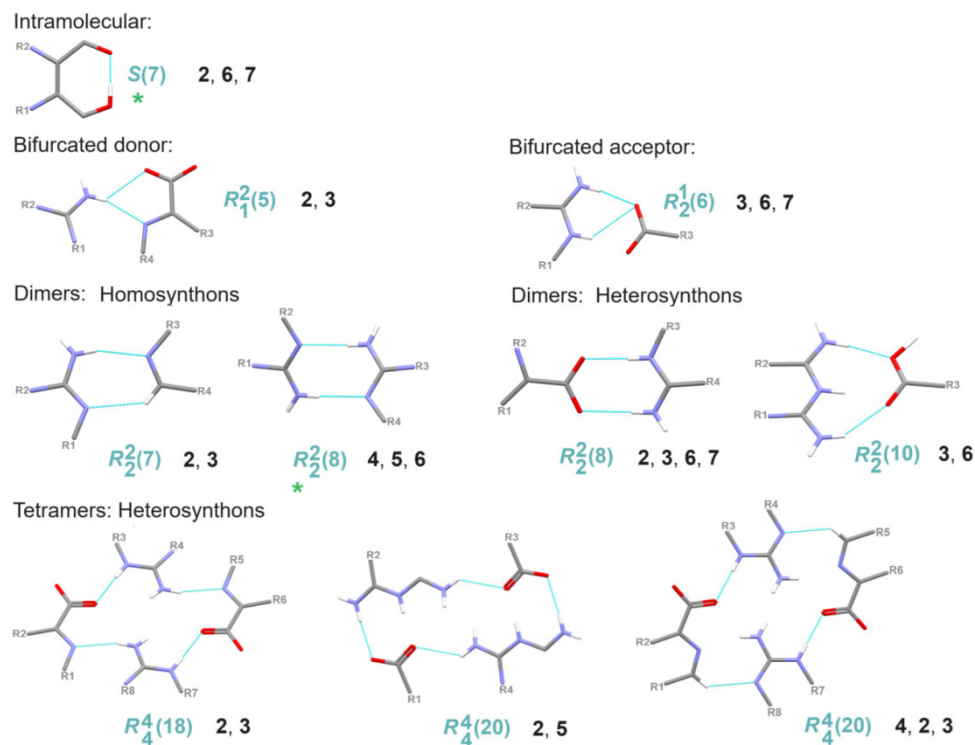
Figure 8. Representative recurrent cyclic supramolecular synthons observed in crystal lattices of **1**–**7**. *—Synthon S(7) and homosynthon R^2_2(8) appear at the first level, while the remaining synthons appear at the second level of supramolecular architectures.
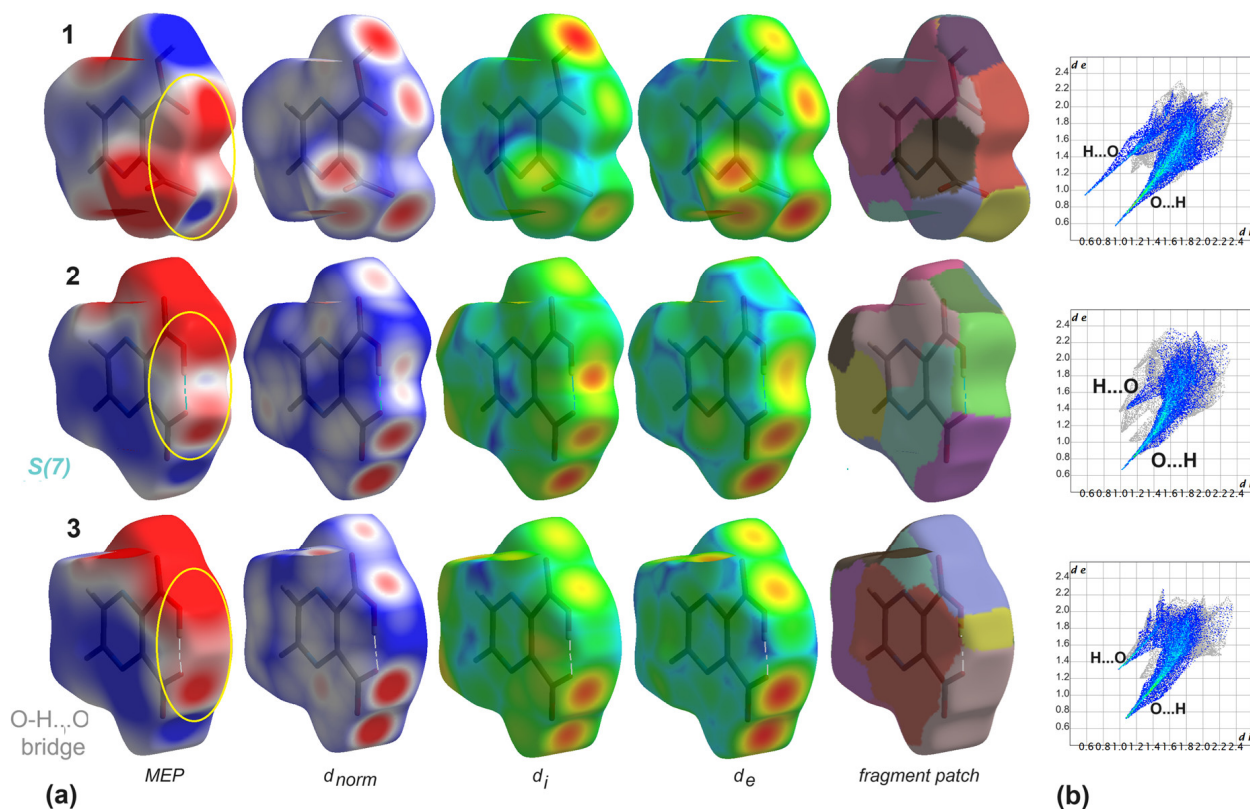
Figure 9. (**a**) Molecular electrostatic potentials (MEP) mapped on the Hirshfeld surfaces and the Hirshfeld surfaces for crystals **1**–**3**; (**b**) fingerprint plots presenting O···H/H···O interactions (yellow circles).

Another appealing issue of our studies concerns other supramolecular motifs formed by weak interactions. In particular, the dual synthon observed in **4** and **5**: here, phenyl participates in the formation of either a supramolecular chain via π···π or classical homodimer *R*22(8) via N-H···N (Figure 10).
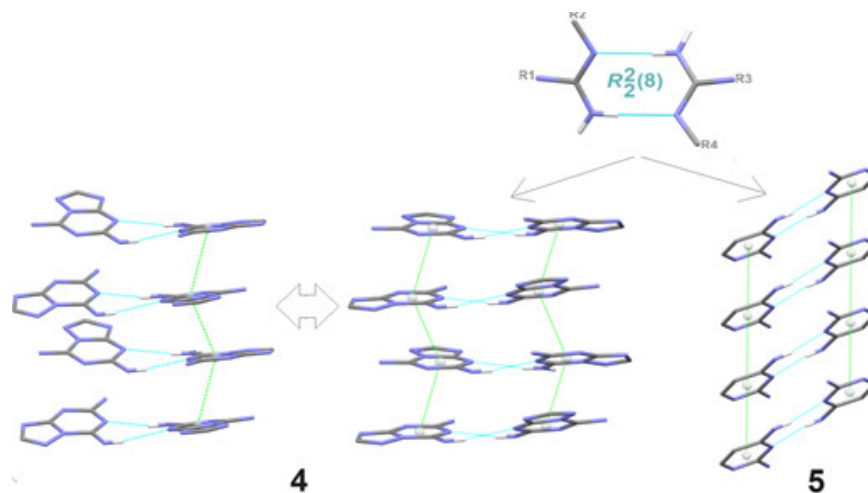
Figure 10. Dual synthon found in **4** and **5**.

With regard to the existence of π···π interactions, we have undertaken a more systematic study of crystal packing to establish more trends using the method of Loots and Barbour [54] and the classification of Desiraju and Gavezzotti [55]. As a consequence, we observed three packing motifs in terms of the relationship between the C···H and C···C interactions. The values were obtained via fingerprint analysis in CrystalExplorer. In particular, structures 2, **3**, and **7** represent the *gamma* motif (with a ratio 1.2–2.7); **4** and **6** structures—the *herringbone* motif (with a ratio greater than 4.5), while structure **5** has a *beta* motif (in the range 0.46–1.0), see Table S10.

3.3. Comparison with Other Carboxy-Pyrazine/Thiophene Crystal Structures Retrieved from the CSD

For comparative purposes in the context of intramolecular interactions, we analyzed similar ones available in CSD crystal structures containing 3-carboxypyrazine-2-carboxylate and 4-carboxythiophene-3-carboxylate anions, such as BEBCET [8], ZIKREQ [7], LOFQIJ [4], LEJRIB [6], DIMNAR [1], MIPWEN [48], VUZYUL [12], LUDTAH [14], NIBPIZ [15], and WUVCUN01[16] (Table S11). The intramolecular O···H···O bridge between neighboring carboxylic groups is observed only in BEBCET and ZIKREQ. Other mentioned 3-carboxypyrazine-2-carboxylate-based structures, such as LOFQIJ [4], LEJRIB [6], DIMNAR [1], MIPWEN [48], and VUZYUL [12], as well as crystals containing 4-carboxythiophene-3-carboxylate, such as LUDTAH [14], NIBPIZ [15], and WUVCUN01 [16], contain the *S*(7) synthon. In this context, the full interaction maps (FIMs) tool was helpful in the examination and visualization of whether intramolecular supramolecular preferences in the corresponding types of crystals are satisfied. FIMs were calculated to predict their preferred interaction behavior in the context of CSD interaction statistical data. The most likely predicted positions of functional groups and differences in landscapes of interactions are visible in Figure 11. Regions of hydrogen bonding donor probabilities are demonstrated in blue, while acceptors are shown in red. Brown spots signify aromatic interactions. The intensity of the colors corresponds to the likelihood of the relevant interactions. The most important aspect is related to the characteristic zones around carboxylic groups which are highly representative of the selected groups: structures with intramolecular O-H···O bridge (see *a*), structures with intramolecular synthon S(7) (*b*), and others (*c*).
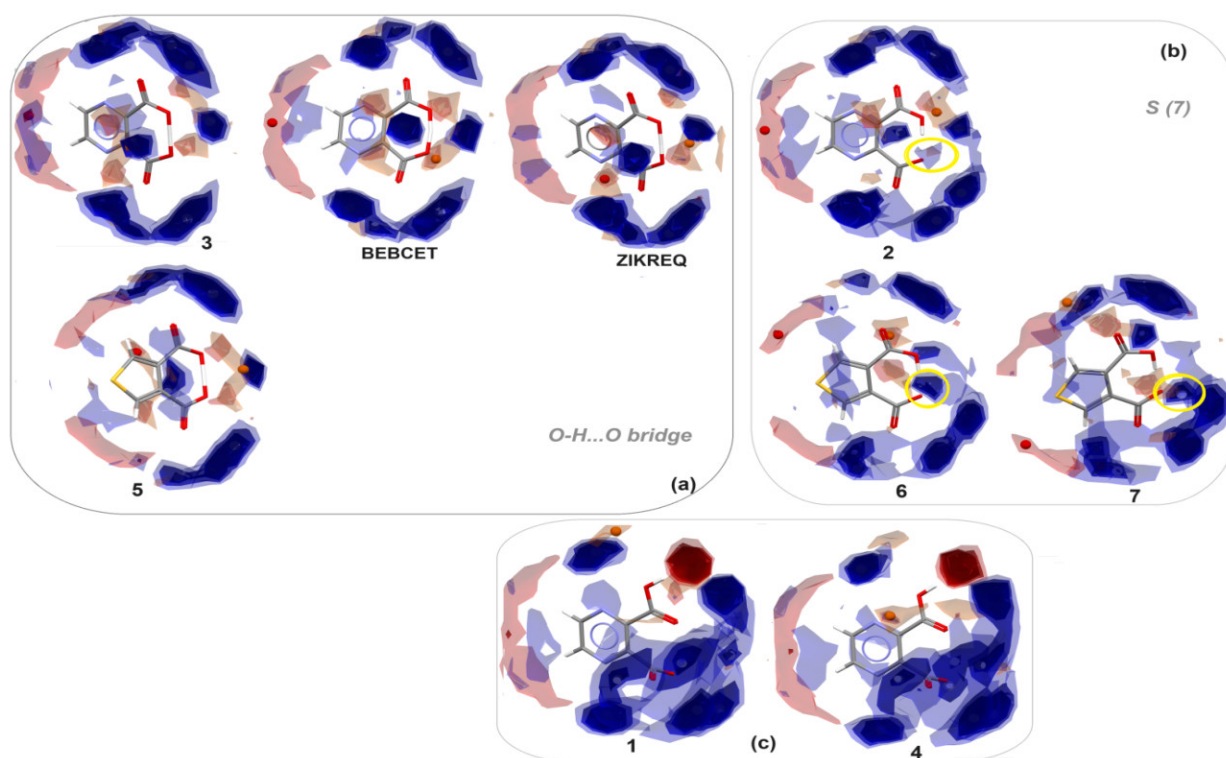
Figure 11. FIMs for analyzed crystals: (**a**,**b**) structures adopting a closed conformation with the O-H⋯O intramolecular bridge (**a**) and the *S*(7) synthon (intramolecular interactions in yellow circles) (**b**); (**c**) structures adopting an open conformation with no intramolecular interactions.

3.4. Intermolecular Interaction Energies and Energy Frameworks

To get insight into the supramolecular landscape of a "whole-of-molecule," we calculated energy frameworks for the model energies of the pairs present in the crystals **1**–**7**. The interaction energy is expressed by the equation:

$$E_{tot} = k_{ele}\, E_{ele} + k_{pol}\, E_{pol} + k_{dis}\, E_{dis} + k_{rep}\, E_{rep}$$

where E_{tot} means total energy, k—scale factor, E_{ele}—electrostatic, E_{pol}—polarization, E_{dis}—dispersion, and E_{rep}—repulsion term [41,45]. The total energy agrees with the quantum mechanical effects at the corresponding theoretical level. The calculated interaction energetics, including the crystallographic symmetry operations, for the selected pairs are presented in Figure 12, Figure 13 and Figures S4–S7, and Table 1. The types of energy terms are distinguished by different colors: red signifies classical electrostatic (the coulombic), green is the dispersion term, and blue is the total energy. The energies are visualized by the "cylinders". The width of these cylinders is proportional to the strength of the interactions. A thorough energy-framework analysis revealed that the dispersion term is dominant in all structures (apart from **3**) due to the high contribution of weak interactions in these crystals. On the contrary, in **3**, the electrostatic term, related to the strong classical interactions, is dominant. In addition, energy frameworks are relevant to the packing of supramolecular motifs. The same motif arrangement in **2** and **3** and in **5** and **6** is noticeable.
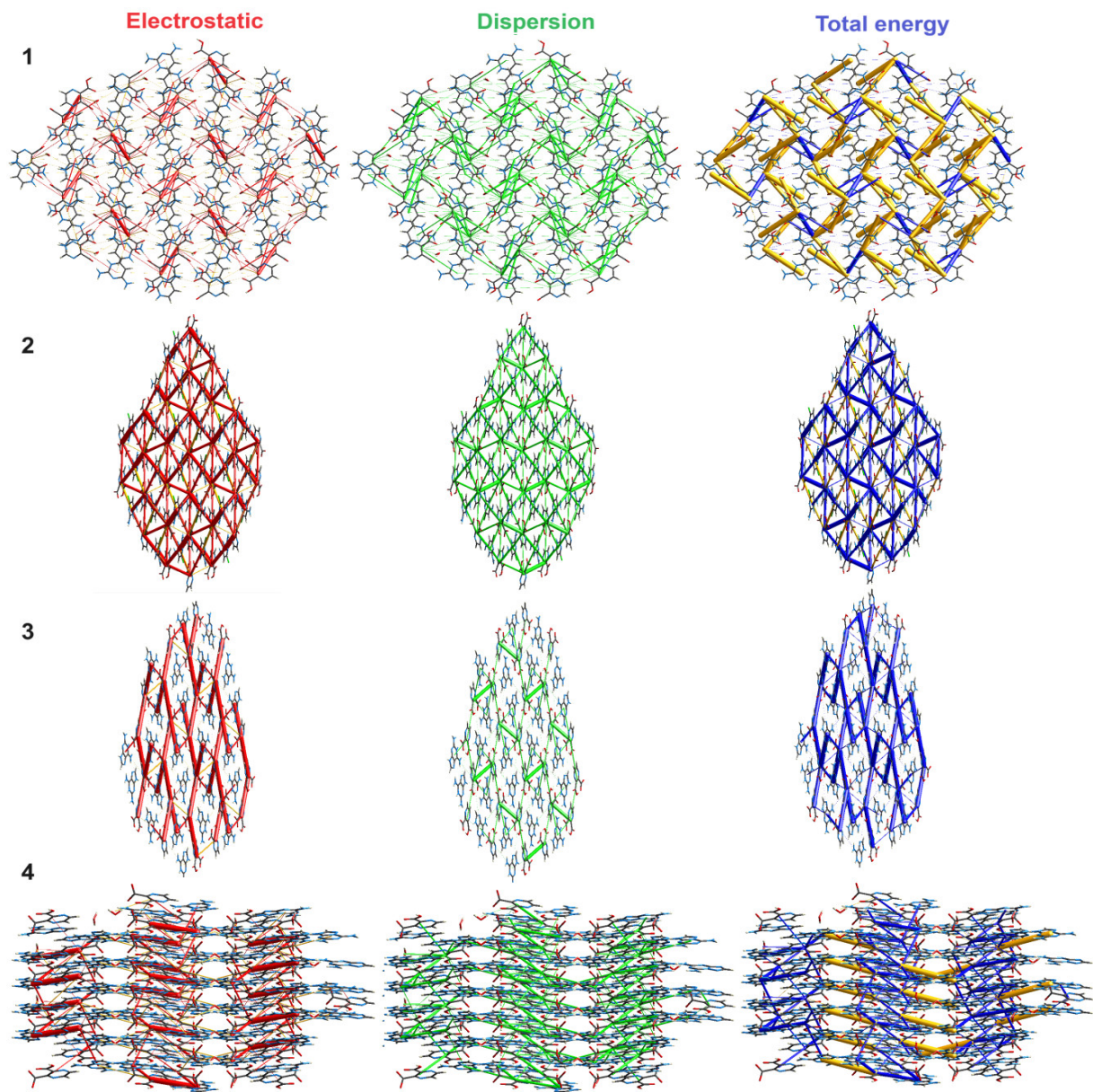
Figure 12. Energy-framework plots for the analyzed compounds **1**–**4**, calculated with Crystal-Explorer [42]. The electrostatic, dispersion energy components, and total energy interactions are presented separately in projection along the a-axis. The tube size is set to 100.
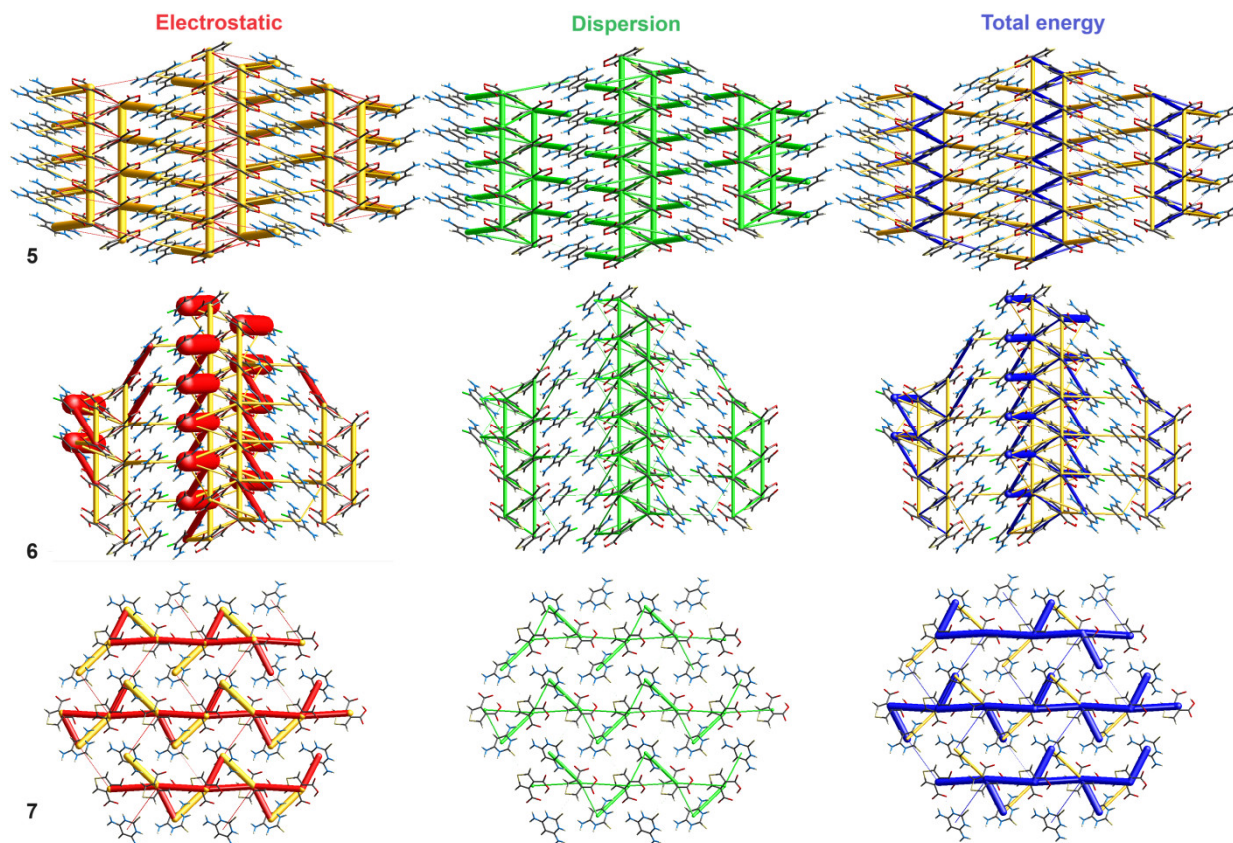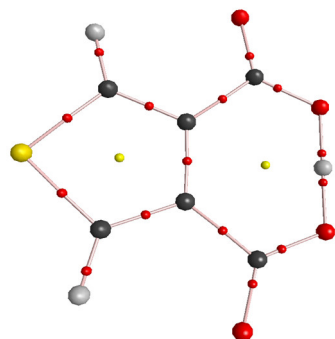
Figure 13. Energy-framework plots for the analyzed compounds **5–7**, calculated with CrystalExplorer [25]. The electrostatic, dispersion energy components, and the total energy interactions are presented separately in projection along the *a*-axis. The tube size is set to 100.

3.5. Quantum Chemical Results

The systems under study contain 4-carboxythiophene-3-carboxylate (**A$^-$**) and carboxypyrazine-2-carboxylate (**B$^-$**) anions. In both anions, intramolecular hydrogen bonding was studied (see Table 2). For clarity, individual atoms are denoted by subscripts that indicate bonded atoms. In **A$^-$** both $O_H \cdots H_O$ distances are comparable and significantly longer than expected, unlike less symmetric **B$^-$**, with one of them being ca. 1.1 Å. This could be ascribed to longer C_{arom}–C_{O2} bond lengths and thus longer $O_H \cdots O_H$ distances and weaker $O_H \cdots H_O$ bonding in **B$^-$**. This agrees with the lower C_{O2}–O_H–H_O angles (almost tetrahedral) in **B$^-$** than in **A$^-$**. This implies a much higher deviation of the O_H–H_O–O_H angle from linearity as well. These geometric suggestions are confirmed by electronic structure data (Table 2, Figures 14 and 15). BCP electron density values show that despite nearly equal C_{O2}–O_H bond strengths in both anions, the shorter O_H–H_O bond in **B$^-$** is significantly stronger than other $O_H \cdots H_O$ interactions. According to the most negative value of the BCP electron density Laplacian, this bond has the highest polar character of covalent bonding (even compared to C_{O2}–O_H bonds). Non-zero BCP ellipticities of $O_H \cdots H_O$ bonds can be mainly ascribed to mechanical strain in cyclic structures, while in significantly stronger C_{O2}–O_H bonds, it is prevailingly caused by their partial π character. The covalent character (see the BCP electron density Laplacian) and π character of the C_{arom}–C_{O2} bonds (see the BCP ellipticity) in **A$^-$** are higher than in **B$^-$**.

There are only vanishing differences between carboxyl C atomic charges (Table 2). Differences in O atomic charges are related to different degrees of their hydrogen bonding (compare the BCP electron densities of the O_H–H_O bonds).

The higher aromaticity of thiophene in comparison with pyrazine [56] causes the higher π character of the adjacent bonds. This causes the higher rigidity of the carboxyl groups in **A$^-$** and lower polarizability of their atoms.

Table 2. Interatomic distances, bond angles, electron density at bond critical point ρ_{BCP}(X-Y), its Laplacian $\nabla^2\rho_{BCP}$(X-Y), ellipticity of X–Y bonds, and atomic charges Q(X) of atom X in model compounds **A$^-$** and **B$^-$**. The subscripts Y denote bonded atoms.

	A$^-$	**B$^-$**
Interatomic distances [Å]		
O_H–H_O	1.186	1.099
	1.202	1.313
$O_H \cdots O_H$	2.388	2.401
C_{O2}–O_H	1.293	1.306
	1.291	1.285
C_{arom}–C_{O2}	1.515	1.530
	1.516	1.536
Bond angles [°]		
O_H–H_O–O_H	178.2	169.7
C_{O2}–O_H–H_O	112.1 (2×)	110.5
		108.9
QTAIM characteristics		
$\rho_{BCP}(O_H$–$H_O)$ [e/bohr^3]	0.1825	0.2349
	0.1749	0.1281
$\nabla^2\rho_{BCP}(O_H$–$H_O)$ [e/bohr^5]	-0.5129	-1.2432
	-0.4257	-0.0388
$\varepsilon_{BCP}(O_H$–$H_O)$	0.010 (2×)	0.008
		0.039
$\rho_{BCP}(C_{O2}$–$O_H)$ [e/bohr^3]	0.3472	0.3363
	0.3484	0.3533
$\nabla^2\rho_{BCP}(C_{O2}$–$O_H)$ [e/bohr^5]	-0.5537	-0.5603
	-0.5520	-0.5440
$\varepsilon_{BCP}(C_{O2}$–$O_H)$	0.092	0.086
	0.094	0.100
$\rho_{BCP}(C_{arom}$–$C_{O2})$ [e/bohr^3]	0.2583	0.2563
	0.2577	0.2529
$\nabla^2\rho_{BCP}(C_{arom}$–$C_{O2})$ [e/bohr^5]	-0.6889	-0.6728
	-0.6855	-0.6568
$\varepsilon_{BCP}(C_{arom}$–$C_{O2})$	0.102 (2×)	0.093
		0.085
Q(O_H) [e]	-1.22 (2×)	-1.27
		-1.23
Q(H_O) [e]	0.67	0.68
Q(C_{O2}) [e]	1.77 (2×)	1.76
		1.77

Figure 14. Molecular graph of **A$^-$** anion (C—black, O—red, S—yellow, H—grey, bond critical points—small red, ring critical points—small yellow).
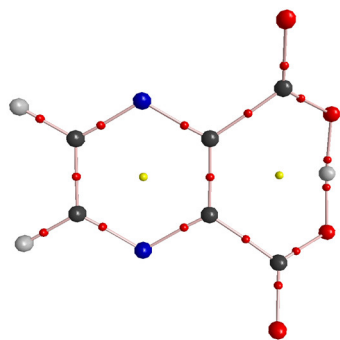
Figure 15. Molecular graph of **B**⁻ anion (C—black, O—red, N—blue, H—grey, bond critical points—small red, ring critical points—small yellow).

4. Conclusions

We successfully synthesized and thoroughly characterized two series of novel salts containing 3-carboxypyrazine-2-carboxylate (structures **1**–**4**) and 4-carboxythiophene-3-carboxylate (**5**–**7**) anions using a wide range of computational methods. The crystal lattices of new species have diverse supramolecular H-bonding motifs generated by O(N,C)-H⋯O, N(C)-H⋯N, N-H⋯S. We recognized recurrent motifs according to the graph-set theory that we next segregated into the hierarchical library. An important observation is that the hydrogen-bonded intramolecular motif $S(7)$ and the robust intermolecular motif $R^2_2(8)$ are present in both series of new salts at the first level of supramolecular architecture. We described π-based supramolecular motifs formed by π⋯πC-O(Cl,S)⋯C intercontacts. In both series of new salts, we identified a dual synthon formed by H-bonding and π-based interactions. In addition, we proved that HS analysis is a suitable tool for the examination and visualization of differences in supramolecular behavior related to intramolecular interactions and proton transfer. According to quantum chemical calculations, it can be concluded that both the O_H⋯H_O intramolecular hydrogen bonds in A⁻ have comparable characteristics, while **B**⁻ contains one classical O_H–H_O bond and one significantly weaker O_H⋯H_O hydrogen bond. Whereas in X-ray structures, the O_H⋯O_H distances are nearly equal in both compounds (*ca.* 2.4 Å), these differences cannot be explained exclusively by longer intramolecular O_H⋯O_H distances in **B**⁻ than in **A**⁻. Therefore, the origin of this behavior should be in the higher aromatic character of the thiophene ring in **A**⁻ than the pyrazine ring in **B**⁻ (see BCP characteristics of the C_{arom}–C_{O2} bonds in Table 2). Consequently, the carboxyl groups in **A**⁻ are more rigid and their O_H atoms less polarizable, which is reflected in the higher equality of both O_H–H_O bond strengths.

CSD. Figure S6. ATR-FTIR spectrum of 1. Figure S7. ATR-FTIR spectrum of 2. Figure S8. ATR-FTIR spectrum of 3. Figure S9. ATR-FTIR spectrum of 4. Figure S10. ATR-FTIR spectrum of 5. Figure S11. ATR-FTIR spectrum of 6. Figure S12. ATR-FTIR spectrum of 7.

Author Contributions: Conceptualization, A.M. and J.B.; methodology, M.B., A.M. and K.Ł.; validation, K.Ł. and J.B.; formal analysis, J.B. and M.B.; investigation, K.Ł., J.B., A.M. and M.B.; data curation, K.Ł. and J.B.; writing—original draft preparation, K.Ł., J.B., M.B. and A.M. All authors have read and agreed to the published version of the manuscript.

Data Availability Statement: CCDC 2364043–2364049 contain the supplementary crystallographic data for this paper, accessed on 20 June 2024. These data can be obtained free of charge via https://www.ccdc.cam.ac.uk/structures.

Conflicts of Interest: The authors declare no conflicts of interest.

References

1. Faizan, M.; Afroz, Z.; Alam, M.J.; Rodrigues, M.H.; Ahmad, S.; Ahmand, A. Structural, vibrational and electronic absorption characteristics of the monohydrate organic salt of 2-amino-5-bromo-6-methyl-4-pyrimidinol and 2,3-pyrazinedicarboxylic acid: A combined experimental and computational study. *J. Mol. Struct.* **2019**, *1177*, 229. [CrossRef]
2. Faizan, M.; Alam, M.J.; Afroz, Z.; Rodrigues, V.H.N.; Ahmad, S. Growth, structure, Hirshfeld surface and spectroscopic properties of 2-amino-4-hydroxy-6-methylpyrimidinium-2,3-pyrazinedicorboxylate single crystal. *J. Mol. Struct.* **2018**, *1155*, 695–710. [CrossRef]
3. Wu, R.; Chen, Z.; Gao, X.; Chen, X.; Jin, S.; He, L.; Chen, B.; Wang, D. Preparation and characterization of eight crystalline supramolecular salts from 4-dimethylaminopyridine and aromatic acids. *J. Mol. Struct.* **2021**, *1246*, 131088. [CrossRef]
4. Clegg, W.; Harrington, R.W.; Knotts, J.A. *CCDC 1937658: Experimental Crystal Structure Determination. 2019 (deposited on 1 July 2019)*; Newcastle University: Newcastle, UK. [CrossRef]
5. Paramban, R.P.; Afroz, Z.; Mondal, P.K.; Sahoo, J.; Chopra, D. Structural insights into salts and a salt polymorph of nitrogen containing small organic molecules. *J. Mol. Struct.* **2018**, *1170*, 141–150. [CrossRef]
6. Lynch, D.E.; Smith, G.; Byriel, K.A.; Kennard, C.H.L.; Whittaker, A.K. Molecular Cocrystals of Carboxylic Acids. XIV. The Crystal Structures of the Adducts of Pyrazine-2,3-dicarboxylic Acid With 4-Aminobenzoic Acid, 3-Hydroxypyridine and 3-Amino-1,2,4-triazole. *Aust. J. Chem.* **1994**, *47*, 309–319. [CrossRef]
7. Smith, G.; Lynch, D.E.; Byriel, K.A.; Kennard, C.H.L. Molecular Co-Crystals of Carboxylic Acids. 22. The Adducts of Pyrazine-2,3-dicarboxylic Acid with 2-Aminobenzoic Acid (1:2) and 3-Aminobenzoic Acid (1:1 Dihydrate). *Acta Cryst. C* **1995**, *51*, 2629. [CrossRef]
8. Das, B.; Srivastava, H.K. Influence of the Local Chemical Environment in the Formation of Multicomponent Crystals of L-Tryptophan with N-Heterocyclic Carboxylic Acids: Unusual Formation of Double Zwitterions. *Cryst. Growth Des.* **2017**, *17*, 3796. [CrossRef]
9. Smith, G.; Wermuth, U.D. Hydrogen-bonding in the structures of the 1:1 salts of isonipecotamide with a set of four polyfunctional monocyclic heteroaromatic carboxylic acids. *Z. Für Krist. Cryst. Mater.* **2012**, *227*, 656. [CrossRef]
10. Smith, G.; Wermuth, U.D.; Healy, P.C.; White, J.M. The 1:1 proton-transfer compound of 8-quinolinol (oxine) with pyrazine-2,3-dicarboxylic acid: 8-hydroxy quinolinium 3-carboxy pyrazine-2-carboxyl ate dihydrate. *Acta Crystallogr. E* **2006**, *62*, o5089–o5091. [CrossRef]
11. Attar Gharamaleki, J.; Derikvand, Z.; Stoeckli-Evans, H. Acridinium 3-carboxypyrazine-2-carboxyl ate. *Acta Crystallogr. E* **2010**, *66*, o2231. [CrossRef]
12. Eshtiagh-Hosseini, H.; Alfi, N.; Mirzaei, M.; Necas, M. 1,4-Diazoniacyclohexane bis-(3-carboxypyrazine-2-carboxylate) dihydrate. *Acta Cryst. E* **2010**, *66*, o2810–o2811. [CrossRef] [PubMed]
13. Ding, A.; Jin, S.; Jin, S.; Guo, M.; Liu, H.; Guo, J.; Wang, D. Nine supramolecular assemblies from 5,7-dimethyl-1,8-naphthyridine-2-amine and carboxylic acids by strong classical H-bonds and other noncovalent associations. *J. Mol. Struct.* **2017**, *1150*, 595–613. [CrossRef]
14. Liu, S.; Zhang, R.; Li, E.; Xu, Q. Crystal structure of diaqua-bis(1,10-phenanthroline)-zinc(II) bis(thiophene-3-carboxy-4-carboxylate) heptahydrate, [Zn(H_2O)_2(C_{12}H_8N_2)_2][(C_6H_3O_4S)_2]*7H_2O, C_{36}H_{40}N_4O_{17}S_2Zn. *Z. Kristallogr. New Cryst. Struct.* **2014**, *229*, 141–142. [CrossRef]
15. Li, Z.-H.; Xue, L.-P.; Li, S.-H.; Wang, J.-G.; Zhao, B.-T.; Kan, J.; Su, W.-P. Bis(pyridyl) ancillary ligands modulated uninodal 4-, 5- and 6-connected Cd(II) coordination polymers based on 3,4-thiophenedicarboxylate linker. *CrystEngComm* **2013**, *15*, 2745–2752. [CrossRef]

16. Li, L.; Guo, J.B.; Wei-Liu, B.; Min-Wen, Y.; Wang, W.; Xia, X.D.; Mu, K. Crystal structure of bis(2,2′-bipyridine-$\kappa^2 N,N'$)-bis(thiophene-3,4-dicarboxylato-$\kappa^2 O,O'$)-cadmium(II), $C_{32}H_{22}CdN_4O_8S_2$. *Z. Kristallogr. New Cryst. Struct.* **2015**, *230*, 323–325. [CrossRef]

17. Chen, S.-J.; Li, S.-H. Crystal structure of tetra-aqua-bis(μ_2-thiophene-3,4-dicarboxylato-$\kappa^4 O,O':O'',O'''$)-bis(thiophene-3-carboxyl-4-carboxylato-$\kappa^1 O$)-bis(1,10- phenantroline-$\kappa^2 N,N'$)disamarium(III), $C_{24}H_{17}N_2O_{10}S_2Sm$. *Z. Kristallogr. New Cryst. Struct.* **2015**, *230*, 259–260. [CrossRef]

18. Li, Z.-H.; Xue, L.-P. Crystal structure of diaqua-bis-(1,10-phenanthroline)-manganese(II) thiophene-3,4-dicarboxylate heptahydrate, $[Mn(H_2O)_2(C_{12}H_8N_2)_2(C_6H_3O_4S)_2]\cdot 7H_2O$, $C_{36}H_{39}MnN_4O_{17}S_2$. *Z. Kristallogr. New Cryst. Struct.* **2012**, *227*, 453–454. [CrossRef]

19. Li, S.-H.; Guo, D.-J.; Zhao, Y. Crystal structure of hexaquamanganese(II) (4-carboxythiophene-3-carboxylate hemihydrate, $C_{12}H_{16}MnO_{16}S_2$. *Z. Kristallogr. New Cryst. Struct.* **2014**, *229*, 349–350. [CrossRef]

20. Nangia, A.K.; Desiraju, G.R. Crystal Engineering: An Outlook for the Future. *Angew. Chem. Int. Ed.* **2019**, *58*, 4100–4107. [CrossRef]

21. Bolla, G.; Srma, B.; Nangia, A.K. Crystal Engineering of Pharmaceutical Cocrystals in the Discovery and Development of Improved Drugs. *Chem. Rev.* **2022**, *122*, 11514–11603. [CrossRef]

22. Seoane, B.; Castellanos, S.; Dikhtiarenko, A.; Kapeijn, F.; Gascon, J. Multi-scale crystal engineering of metal organic frameworks. *Coord. Chem. Rev.* **2016**, *307*, 147–187. [CrossRef]

23. Allendorf, M.D.; Stavila, A. Crystal engineering, structure–function relationships, and the future of metal–organic frameworks. *CrystEngComm* **2015**, *17*, 229–246. [CrossRef]

24. Rimer, J.D.; Chawla, A.; Le, T.T. Crystal Engineering for Catalysis. *Annu. Rev. Chem. Biomol. Eng.* **2018**, *9*, 283–309. [CrossRef] [PubMed]

25. Bojarska, J.; Łyczko, K.; Mieczkowski, A. Synthesis, Crystal Structure and Supramolecular Features of Novel 2,4-Diaminopyrimidine Salts. *Crystals* **2024**, *14*, 133. [CrossRef]

26. Bojarska, J.; Łyczko, K.; Mieczkowski, A. Novel Salts of Heterocyclic Polyamines and 5-Sulfosalicylic Acid: Synthesis, Crystal Structure, and Hierarchical Supramolecular Interactions. *Crystals* **2024**, *14*, 497. [CrossRef]

27. Groom, C.R.; Bruno, I.J.; Lighfoot, M.P.; Warda, S.C. The Cambridge Structural Database. *Acta Crystallogr. B* **2016**, *72*, 171–179. [CrossRef]

28. Dolzhenko, A.V.; Dolzhenko, A.V.; Chui, W.-K. Synthesis of 5,7-diamino[1,2,4]triazolo[1,2-*a*][1,3,5]triazines *via* annulation of 1,3,5-triazine ring onto 3(5)-amino-1,2,4-triazoles. *Heterocycles* **2007**, *71*, 429–436. [CrossRef]

29. Sheldrick, G.M. Crystal Structure Refinement with SHELXL. *Acta Cryst. C* **2015**, *71*, 3–8. [CrossRef]

30. Dolomanov, O.V.; Bourhis, L.J.; Gildea, R.J.; Howard, J.A.K.; Puschmann, H. OLEX2: A complete structure solution, refinement and analysis program. *J. Appl. Crystallogr.* **2009**, *42*, 339–341. [CrossRef]

31. Macrae, C.F.; Sovago, I.; Cottrell, S.J.; Galek, P.T.A.; McCabe, P.; Pidcock, E.; Platings, M.; Shields, G.P.; Stevens, J.S.; Towler, M.; et al. Mercury 4.0: From visualization to analysis, design and prediction. *J. Appl. Cryst.* **2020**, *53*, 226–235. [CrossRef] [PubMed]

32. Spek, A.L. Structure Validation in chemical crystallography. *Acta Cryst. D* **2009**, *65*, 148–155. [CrossRef] [PubMed]

33. Frisch, M.J.; Trucks, G.W.; Schlegel, H.B.; Scuseria, G.E.; Robb, M.A.; Cheeseman, J.R.; Scalmani, G.; Barone, V.; Mennucci, B.; Petersson, G.A.; et al. *Gaussian 09, version D.01*; Gaussian Inc.: Wallingford, CT, USA, 2011.

34. Parr, R.G.; Wang, W. *Density-Functional Theory of Atoms and Molecules*; Oxford University Press: New York, NY, USA, 1994.

35. Head-Gordon, M.; Pople, J.A.; Frisch, M.J. MP2 energy evaluation by direct methods. *Chem. Phys. Lett.* **1988**, *153*, 503–506. [CrossRef]

36. Head-Gordon, M.; Head-Gordon, T. Analytic MP2 Frequencies Without Fifth Order Storage: Theory and Application to Bifurcated Hydrogen Bonds in the Water Hexamer. *Chem. Phys. Lett.* **1994**, *220*, 122–128. [CrossRef]

37. Bader, R.F.W. *Atoms in Molecules: A Quantum Theory*; Clarendon Press: Oxford, UK, 1990; ISBN 9780198558651.

38. Biegler-König, F.; Schönbohm, J.; Bayles, D. AIM2000—A Program to Analyze and Visualize Atoms in Molecules. *J. Comput. Chem.* **2001**, *22*, 545–559. [CrossRef]

39. McKinnon, J.J.; Jayatilaka, D.; Spackman, M.A. Towards quantitative analysis of intermolecular interactions with Hirshfeld surfaces. *Chem. Commun.* **2007**, *37*, 3814–3816. [CrossRef] [PubMed]

40. Spackman, M.A.; Jayatilaka, D. Hirshfeld surface analysis. *CrystEngComm* **2009**, *11*, 19–32. [CrossRef]

41. Spackman, P.R.; Turner, M.J.; McKinnon, J.J.; Wolff, S.K.; Grimwood, D.J.; Jayatilaka, D.; Spackman, M.A. CrystalExplorer: A program for Hirshfeld surface analysis, visualization and quantitative analysis of molecular crystals. *J. Appl. Crystallogr.* **2021**, *54*, 1006–1011. [CrossRef] [PubMed]

42. Turner, M.J.; McKinnon, J.J.; Wol, S.K.; Grimwood, D.J.; Spackman, P.R.; Jayatilaka, D.; Spackman, M.A. *CrystalExplorer, version 3.1*; The University of Western Australia: Perth, Australia, 2017.

43. Allen, F.H.; Kennard, O.; Watson, D.G.; Brammer, L.; Orpen, A.G.; Taylor, R. Tables of Bond Lengths determined by X-Ray and Neutron Diffraction. Part 1. Bond Lengths in Organic Compounds. *J. Chem. Soc. Perkin Trans.* **1987**, *2*, S1–S19. [CrossRef]

44. Jayatilaka, D.; Grimwood, D.J. Tonto: A Fortran Based Object-Oriented System for Quantum Chemistry and Crystallography. In Proceedings of the International Conference on Computational Science 2003, Petersburg, Russia, 2–4 June 2003; pp. 142–151. [CrossRef]

45. Mackenzie, C.F.; Spackman, P.R.; Jayatilaka, D.; Spackman, M.A. CrystalExplorer model energies and energy frameworks: Extension to metal coordination compounds, organic salts, solvates and open-shell systems. *IUCrJ* **2017**, *4*, 575–587. [CrossRef] [PubMed]
46. Jelsch, C.; Ejsmont, K.; Huder, L. The enrichment ratio of atomic contacts in crystals, an indicator derived from the Hirshfeld surface analysis. *IUCrJ* **2014**, *1*, 119–128. [CrossRef] [PubMed]
47. Wood, P.A.; Olsson, T.S.G.; Cole, J.C.; Cottrell, S.J.; Feeder, N.; Galek, P.T.A.; Groom, C.R.; Pidcock, E. Evaluation of Molecular Crystal Structures Using Full Interaction Maps. *CrystEngComm* **2013**, *15*, 65–72. [CrossRef]
48. Smith, G.; White, J.M. Short Communication: Molecular Cocrystals of Carboxylic Acids: The Preparation of the 1:1 Proton-Transfer Compounds of Creatinine with a Series of Aromatic Acids and the Crystal Structure of that with Pyrazine-2,3-dicarboxylic Acid. *Aust. J. Chem.* **2001**, *54*, 97–100. [CrossRef]
49. Kitaigorodskii, A.I. *Organic Chemical Crystallography*; Consultants Bureau: New York, NY, USA, 1961; pp. 1–30, 65–112.
50. Kitaigorodskii, A.I. *Molecular Crystals and Molecules*; Academic Press: London, UK, 1973; pp. 1–133.
51. Etter, M.C. Encoding and decoding hydrogen-bond patterns of organic compounds. *Acc. Chem. Res.* **1990**, *23*, 120–126. [CrossRef]
52. Bernstein, J.; Davis, R.E.; Shimoni, L.; Chang, N.L. Patterns in Hydrogen Bonding: Functionality and Graph Set Analysis in Crystals. *Angew. Chem. Int. Ed. Engl.* **1995**, *34*, 1555–1573. [CrossRef]
53. Drebushchak, T.N.; Drebushchak, N.A.; Pankrushina, N.A.; Boldyreva, E.V. Single-crystal to single-crystal conformational polymorphic transformation in tolbutamide at 313 K. Relation to other polymorphic transformations in tolbutamide and chlorpropamide. *CrystEngComm* **2016**, *18*, 5736–5743. [CrossRef]
54. Loots, L.; Barbour, L.J. A simple and robust method for the identification of π–π packing motifs of aromatic compounds. *CrystEngComm* **2012**, *14*, 300–304. [CrossRef]
55. Desiraju, G.R.; Gavezzotti, A. Crystal structures of polynuclear aromatic hydrocarbons. Classification, rationalization and prediction from molecular structure. *Acta Cryst. B* **1989**, *B45*, 473–482. [CrossRef]
56. Finkelstein, P.; Gershoni-Poranne, R. An Additivity Scheme for Aromaticity: The Heteroatom Case. *ChemPhysChem* **2019**, *20*, 1508–1520. [CrossRef] [PubMed]